Vortex Dynamics
From Physical to Mathematical Aspects

Edited by İlkay Bakırtaş and Nalan Antar

Vortex Analysis and Fluid Transport in Time-Dependent Flows

Stefania Espa, Maria Grazia Badas and Simon Cabanes

Abstract

In this contribution, we present a set of procedures developed to identify fluid flow structures and characterize their space-time evolution in time-dependent flows. In particular, we consider two different contests of importance in applied fluid mechanics: 1) large-scale almost 2D atmospheric and oceanic flows and 2) flow inside the left ventricle in the human blood circulation. For both cases, we designed an ad hoc experimental model to reproduce and deeply investigate the considered phenomena. We will focus on the post-processing of high-resolution velocity data sets obtained via laboratory experiments by measuring the flow field using a technique based on image analysis. We show how the proposed methodologies represent a valid tool suitable for extracting the main patterns and quantify fluid transport in complex flows from both Eulerian and Lagrangian perspectives.

Keywords: pattern identification, laboratory experiments, image analysis, rotating turbulence, flow in the left ventricle

1. Introduction

In most of the fluid flows of interest in nature and technology (i.e., geophysical flows, blood flow in the human circulation as well as flows in turbomachinery and around vehicles) the presence of turbulence in normally observed; therefore, their reproducibility and repeatability have always represented a crucial issue. In this regard, it is widely recognized that laboratory experiments represent a valid tool for the simulation and investigation of complex fluid flows under controlled conditions. With the improvement of measuring techniques, the possibility of acquiring huge high-resolution data sets in space and time is continually increasing. It is then fundamental to consider procedures suitable for a proper analysis of these data aimed at the definition and the characterization of the main flow pattern and of their evolution. In this contribution, we consider two examples of different contests of importance in applied fluid mechanics: 1) β-plane turbulence in the framework of large-scale almost 2D atmospheric and oceanic flows and 2) effect of artificial valves on the flow in the left ventricle in the framework of an in vitro model of human blood circulation. In both cases, the complexity of the flow arises from the embedded non-linear phenomena i.e., interaction of structures at different scales, the interplay between vortices waves and turbulence, anisotropy in the energy

transfers, and in transport phenomena. Due to chaotic advection, the Lagrangian motion of passive particles can be very complex even in regular, i.e., non-turbulent, flow fields [1] as in the situations here discussed in which we considered almost 2D and time-periodic velocity fields. The chapter is organized as follows. In Section 2, we describe the case studies and the considered experimental apparatus. Theory, its application to the experiments, and the different post-processing methodology are described in Section 3, Section 4 contains some results. We discuss and give our conclusions in Section 5.

2. Material and methods

We provide below the description of the experimental models designed to reproduce: 1) turbulent flows affected by a β-effect, 2) the flow downstream a natural/artificial valve in the left ventricle as well as an overview of the technique used to measure the velocity fields.

2.1 Rotating turbulent flows with a β-effect

In rotating turbulent flows, the latitudinal variation of the Coriolis parameter, the so-called β-effect, may redirect the upward energy flux towards the zonal modes thus inducing the anisotropization of the inverse energy cascade, typically observed in large-scale geophysical flows. Due to the combined effects of planetary rotation, topographical constraints, and fluid stratification, these circulations can be assumed quasi-two-dimensional to the first degree of approximation. Actually, the anisotropic inverse energy cascade represents one of the leading causes for the formation and maintenance of jet-like structures along the zonal direction, the so-called zonation [2–5] observed in the atmospheres of the Giant Planets and in the terrestrial oceans. These environments are characterized by the existence of a banded structure, i.e., eastward and westward zonal flows, as well as by the coexistence of turbulence and waves on all scales [6].

In this contest, in addition to the characteristic scales of 2D turbulence [7] associated with the small-scale forcing k_f and the large-scale friction k_{fr}, two more wavenumbers have to be considered: the Rhines wavenumber k_{Rh} and the transitional wavenumber k_β. The Rhines wavenumber is defined as the scale at which the velocity root-mean-square U_{RMS} is equal to the phase speed of Rossby waves $k_{Rh} = (\beta/2U_{RMS})^{1/2}$ [2] and can be related to the meridional size of the jet. If the flow is continuously forced at small scales and at a constant rate ε, the balance between the eddy characteristic time and the Rossby wave period exists in correspondence of $k_\beta = (\beta^3/\varepsilon)^{1/5}$, i.e., the so-called anisotropic transitional wavenumber which characterizes the threshold of the inverse cascade anisotropization [8]. The ratio between the transitional wavenumber and the Rhines wavenumber provides the non-dimensional number, $R_\beta = k_\beta/k_{Rh}$, known as the zonostrophy index. This represents a key parameter in turbulent flows subjected to a β-effect, since it discerns different flow regimes of the so-called β-plane turbulence. Indeed $R_\beta < 1.5$ pertains to flows with strong large-scale friction (friction dominated regime), in the range $1.5 < R_\beta < 2.5$ a flow shows a transitional behavior, and for $R_\beta > 2.5$ a flow develops within the regime of zonostrophic turbulence [8].

To deeply investigate these features, we carried out several experimental campaigns in a rotating tank facility available at the Hydraulics Laboratory of the Sapienza University of Rome. As reported in previous papers [9, 10], the

experimental setup consists of a square tank 1 m in diameter placed on a rotating table whose imposed rotation is counter-clockwise in order to emulate flows in the Northern hemisphere of a planet. To simulate the dynamics associated with the latitudinal variation of the Coriolis parameter in the Polar Regions, we consider the effects induced by the parabolic shape assumed by the free surface of a rotating fluid. In fact, it is represented by a quadratic variation in r, being r the radial distance from the pole and assuming the pole as the reference point (polar β-plane or γ plane approximation) [10, 11]. In this model, the center of the tank (i.e., the point of maximum depression of the fluid surface) represents the pole, while the periphery of the domain corresponds to lower latitudes.

In particular, a local Cartesian frame of reference at the midlatitude of the tank ($r_m = R/2$; where R is the radius of the tank) was considered to evaluate the strength of the β term in each experiment [9]. We run a huge set of experiments by changing the main parameters of the flow, i.e. the rotation rate of the system, the fluid thickness, the amount of energy introduced into the system as well as the forcing characteristics [12–15]. Here, we focus on the analysis of the flow induced by a localized forcing, i.e. the formation of a single eastward/westward jet. To this aim, we consider an electromagnetic forcing obtained with the Lorentz force arising from the interaction of a horizontal electric field and a vertical magnetic field.

We perform a set of runs in which the magnets are located along an arc of latitude in the range $180° < \varphi < 360°$ at a distance $r = 17$ cm from the pole; the considered angular velocity and fluid depth at rest are $\Omega = 3\,\text{rads}^{-1}$ and $H_0 = 4$ cm, respectively. To force the flow, we considered the same orientation of polarity chosen such as to introduce an eastward/westward momentum and facilitate the formation of an eastward/westward zonal jet; in fact, the stationary position of the magnets locked the jet's location. In each of these runs, we vary the intensity of the current in the range $2A \leq I \leq 6A$; the forcing was continuously applied for all the duration of the experiments.

2.2 Flow in the left ventricle in the human blood circulation

The overall functionality of the heart pump is strongly related to the intraventricular flow features. Complexity in the ventricular flow is mainly due to fluid-wall interactions and turbulence onset in correspondence of the boundaries, three-dimensionality, and asymmetry in the pattern development. Here, the focus is on the investigation of the flow in the left ventricle (LV) during a cardiac cycle: it consists of an intense jet forming downstream of the mitral valve and in the development of the related coherent structures i.e., a vortex ring, which grows up during the systole, impinges on the ventricle walls and vanishes almost completely during the systole. A deeper analysis of the flow pattern evolution has shown on one hand that the observed flow structure appears to be favorable to ejection through the aortic valve during the systole [16] and on the other hand the mutual relationships between the formation and development of coherent structures in the LV and its functionality. Actually, one of the main reasons for the deviation from physiological conditions is represented by the replacement of the mitral valve with a prosthetic one, which obviously causes deep modifications in the hemodynamics and, consequently, in the associated flow pattern [17–19].

We reproduce in the laboratory the ventricular flow by means of a pulse duplicator widely described in previous papers [19–21], below we summarize its working principle. A flexible, transparent sack made of silicone rubber (wall

thickness ~ 0.7 mm) simulates the LV allowing at the same time for the optical access. The model ventricle is fixed on a circular plate, 56 mm in diameter, and connected to a constant-head tank by means of two Plexiglas conduits. Along the outlet (aortic) conduit a check valve was mounted, whereas different types of valves were placed on the inlet (mitral) orifice.

We consider three different scenarios: a) the inlet was designed in order to obtain a uniform velocity profile at the orifice mimicking physiological conditions, b) a monoleaflet (Bjork–Shiley monostrut) in mitral position 3) a bileaflet bicarbon prosthetic valve in mitral position; both valves were 31 mm in nominal diameter. The model of the LV was placed in a rectangular tank with Plexiglas (transparent) walls; its volume changed according to the motion of the piston, placed on the side of the tank. The piston was driven by a linear motor, controlled by means of a speed-feedback servo-control. The motion assigned to the linear motor was tuned to reproduce the volume change by clinical data acquired in vivo by echo-cardiography on a healthy subject [20].

2.3 Measuring technique

Two-dimensional velocity fields are measured by means of an image analysis technique called Feature Tracking, FT [22, 23]. The measurement chain can be summarized in the following steps: 1) identification of a proper measurement plane in the fluid domain; 2) seeding of the working fluid with a passive tracer; 3) illumination of the measurement plane previously identified; 4) image acquisition; 5) image pre-processing of the acquired images; 6) particle detection and temporal tracking to isolate particles and track them in consecutive frames; 7) data post-processing to obtain the relevant flow parameters. Obviously, flow images are acquired at a certain space–time resolution, depending on the characteristic time and length scales of the investigated phenomena, the details for each apparatus are provided in the corresponding subsection.

Pre-processing includes the sequence of operations carried out to improve the quality of acquired images for the subsequent core of the processing phase. Basically, the procedure implies the background removal as well as the removal of parts of the image which are not significant for the flow analysis as for instance regions close to the boundaries. In fact, the glares due to the interaction between the lighting system and the domain walls may affect the processing algorithm.

FT is a multi-frame algorithm based on the assumption of image light intensity conservation in space and time between two successive frames and in the neighborhood of the seeding particles; this assumption holds for small time intervals. The algorithm essentially considers measures of correlation windows between successive frames and evaluates displacements by considering the best correspondence (in terms of a defined matching measure) of selected interrogation windows between subsequent images. Sparse velocity vectors are then obtained by dividing the displacement by the time interval between two frames; FT then provides a Lagrangian description of the velocity field. These sparse data can be interpolated on a regular grid through a resampling procedure allowing for the reconstruction of the instantaneous and time-averaged Eulerian velocity fields as well. The advantage of having at the same time both the Lagrangian and the Eulerian description of the flow is evident; in addition, if compared to other tracking algorithms, FT is not constrained by low seeding density, so it provides accurate displacement vectors even when the number of tracer particles within each image is very large [22].

3. Data analysis

3.1 Traveling waves and eddies

As mentioned before, in these jet flows waves and eddies co-exist; to highlight the propagation of the traveling structures in the physical space, we consider both a measure based on Hovmöller diagrams and the theoretical phase speed of the Rossby wave.

As for the former, we map the time evolution of the stream function ψ as a function of φ at different radius, and in particular in correspondence of $r = r_{MS}$, i.e., the radius where the radial shear is a maximum. The diagrams may show linear features with negative or positive slopes, indicating westward/eastward propagating structures; the propagating structures could be waves or eddies, or both. To calculate the propagation velocity V_p in correspondence of a radius r we estimate the slope $\Delta\varphi/\Delta t$ of the contour lines in the azimuthal diagrams:

$$V_p = r\frac{\Delta\varphi}{\Delta t} \tag{1}$$

then the net speed of the propagating structures is evaluated by subtracting the mean zonal velocity from V_p:

$$V_{pn} = V_p - \langle V_z \rangle_\varphi \tag{2}$$

where $\langle V_z \rangle_\varphi$ is the mean zonal velocity averaged over a range of φ corresponding to the forced sector and time interval of $\sim$300 s.

As for the theoretical speed, we have shown in [14] how to derive the dispersion relation of a linear Rossby wave in polar coordinates; here, we reported the final expression:

$$V_t = U - \beta\frac{R^2}{\alpha^2} \tag{3}$$

being R the radius of the device (in this case the radius of the circle inscribed in the square tank), U the average zonal velocity in correspondence of the chosen radius r, and α the coefficient of the Bessel Fourier decomposition, depending on the geometry of the system and on the width of the forced sector and the characteristic of the forcing.

In oceanography, one of the most popular methods used to detect coherent long-lived coherent structures, such as mesoscale eddies, is based on the estimation of the Okubo-Weiss parameter [24, 25]. This quantity describes the relative dominance of deformation with respect to rotation of the flow and it is defined as:

$$OW = s_n - s_s - \omega^2 \tag{4}$$

where $s_n = u_x - v_y$ and $s_s = v_x + u_y$ are the normal and shear components of strain, respectively, $\omega = v_x - u_y$ is vorticity. The subscripts $()_x$ and $()_y$ indicate partial differentiation of the horizontal velocities (u and v) in the x and y directions, respectively. In order to distinguish regions characterized by different topology within the flow domain, one has first to fix a positive threshold OW_0 of the Okubo-Weiss parameter. Then, according to it, the domain can be divided into zones corresponding to vortex cores ($OW < -OW_0$), organized structures surrounding vortex cores ($OW > OW_0$), and the background field ($|OW| \leq OW_0$). A value typically assumed for the threshold is $OW_0 = 0.2\sigma_{OW}$, where σ_{OW} is the standard deviation of OW parameter [26, 27].

3.2 Finite-time Lyapunov exponents and Lagrangian coherent structures

Finite-Time Lyapunov Exponents (FTLE) represents a powerful tool suitable to track coherent structures and to unveil their connections to energetic and mixing processes, in fact, it has been used extensively in different contexts, including biological and geophysical flows [28, 29]. Basically, the FTLE measure the maximum linearized growth rate of the distance among initially adjacent particles tracked over a finite integration time. In brief, the computation of FTLE follows from the definition of the flow map $\Phi(x)_t^{t+T^*}$ over a finite time interval T^*:

$$\Phi(x)_t^{t+T^*} : \quad x(t) \to x(t + T^*) \tag{5}$$

mapping a material point x(t) at time t to its position at t + T^* along its trajectory. After linearization, the amount of stretching about a trajectory is defined in terms of the Cauchy-Green deformation tensor by the matrix:

$$\Delta = \left(\frac{d\Phi(x)_t^{t+T^*}}{dt}\right)^2 \tag{6}$$

Since the maximum stretching occurs when the initial separation is aligned with the maximum eigenvalue of Δ, the FTLE is defined as:

$$\sigma(x, t, T^*) = \frac{1}{|T^*|} \ln \sqrt{\lambda_{max}} \tag{7}$$

Where λ_{max} is the maximum eigenvalue of Δ and $\sqrt{\lambda_{max}}$ corresponds to the maximum stretching factor. In particular, if a positive time interval is considered, the FTLEs measure separation forward in time, thus identifying repelling structures. On the contrary, if negative time intervals are considered, FTLEs measure separation backward in time, thus highlighting attracting structures [28, 30].

In addition, Lagrangian Coherent Structures (LCS) can be inferred from FTLE, [31]. LCS analysis represents a very powerful tool in cardiovascular fluid dynamics [32]; allowing for the identification of stagnant fluid areas, which are associated with an increased risk of thrombus as well as with blood cell damage. In addition, it helps to discern the regions directly affected by the vortices within the fluid domain and, possibly, their, modifications related to pathologies. FTLE investigation was successfully applied to the analysis of data sets obtained from both numerical simulations [27] and in vitro study [33] of a mechanical heart valve, as well as for the in vitro investigation of coherent structures educed from two-dimensional velocity fields in a LV model [21]. Recently, FTLE is also being used in the analysis of data sets collected in vivo [34, 35] and have been recognized as one of the main methods for the analysis of Lagrangian transport in blood flows [36, 37].

4. Results and discussion

4.1 Rotating flows affected by a β-effect

Before running each experiment, the fluid surface is seeded with styrene particles (mean size d_m = 50 μm) acting as passive tracers and the fluid surface is lighted with two lateral lamps. The rotation rate of the table is then raised up to the chosen value and, once the solid body rotation is established, the forcing is switched on, and flow

images are acquired at 20fps by a high-resolution video camera (1023x1240 pixels) co-rotating with the system, perpendicular to the tank and with the optical axis parallel to the rotation axis. FT allows to reconstruct particle trajectories i.e., to provide a description of the flow in a Lagrangian framework; once the instantaneous sparse velocity vectors have been detected, they are interpolated onto a regular grid. In this case, it was convenient to choose a polar coordinate (r, φ) system with the pole corresponding to the center of the tank: the azimuthal direction φ identifies points with the same fluid depth (the so-called zonal direction) and at constant radius r. Sparse data have then been rearranged on a polar grid with 120 radii and 60 circles using a standard cubic spline interpolation procedure. The non-dimensional parameters of importance in our model are: the aspect ratio i.e., the ratio between the horizontal and vertical dimension of the flow domain $H_0/L < <1$ (shallow fluid); the Ekman number Ek $= \nu /\Omega H_0^2$ is order $O(10^{-4})$, ν is the kinematic viscosity; the Rossby number Ro $= U/2\Omega L$ order $O(10^{-3})$, U is the velocity scale; the Reynolds number Re $= Ul_v/\nu$ is order $O(10^2)$, l_v is the characteristic length scale of the eddies. We summarize here some of the main results obtained in the characterization of eastward/westward flows, hereafter indicated as EW and WW case.

4.1.1 Waves and eddies propagation

In **Figures 1** and **2** we plot the instantaneous and time-averaged flow fields obtained in one run (I = 4A) of the experiments WW and EW; the plots are shown hereafter refer to experiments performed using the same forcing amount. **Figure 1** clearly shows a meandering jet squeezed between westward propagating eddies in the instantaneous flow field; on the contrary, the averaged field reveals strong alternating zonal jets and no eddies. These experimental features resemble ocean observations that highlight numerous westward propagating eddies on short time scales [12]. At the difference, the eastward jet is not associated with eddy shedding and traveling structures and the instantaneous and averaged flow appear to be rather similar (**Figure 2**).

To characterize the traveling structure observed in the WW case, we map the velocity stream function ψ as a function of time t and longitude φ in correspondence of the radius of maximum radial shear, r_{MS} (**Figure 3**). In fact, in [14] we were able to demonstrate that the best match between the theoretical and experimental estimation of the speed of propagating structures is found in the correspondence of this radius. To emphasize this aspect, we plot in **Figure 4**, from left to right: the
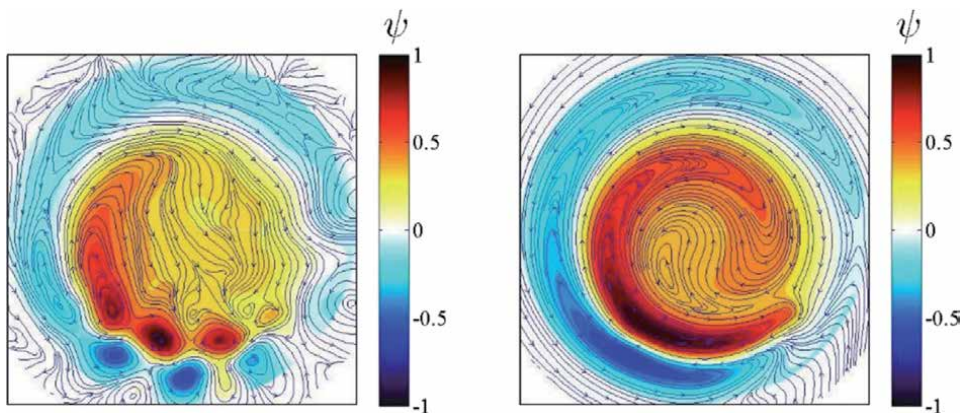

Figure 1.
Instantaneous (left) and time mean (right) normalized stream function superimposed on the streamlines for a WW flow.
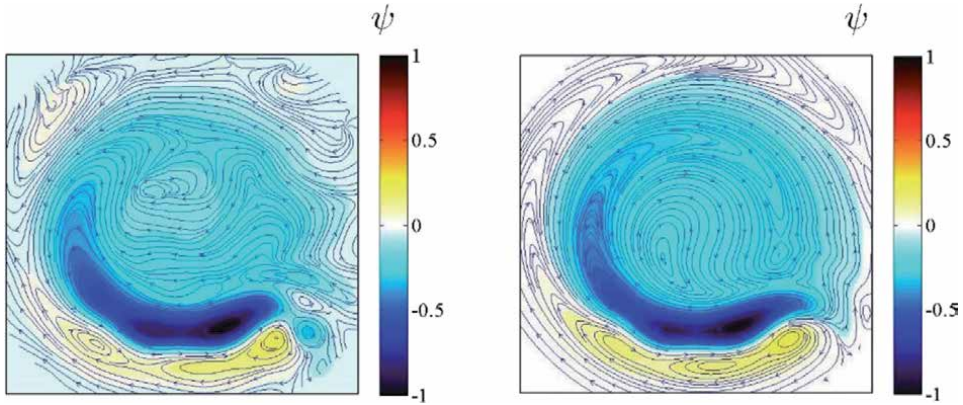
Figure 2.
Instantaneous (left) and time mean (right) normalized stream function superimposed on the streamlines for a EW flow.
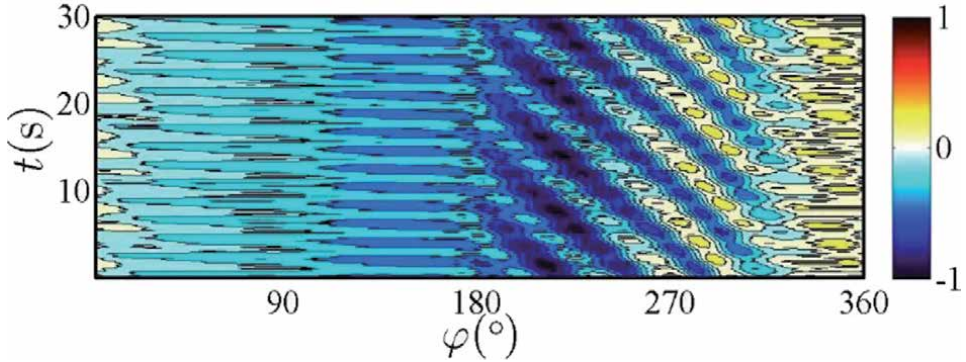

Figure 3.
Azimuthal Hovmöller diagram of the stream function ψ with the radius of the maximum radial shear chosen as the reference radius, WW flow.
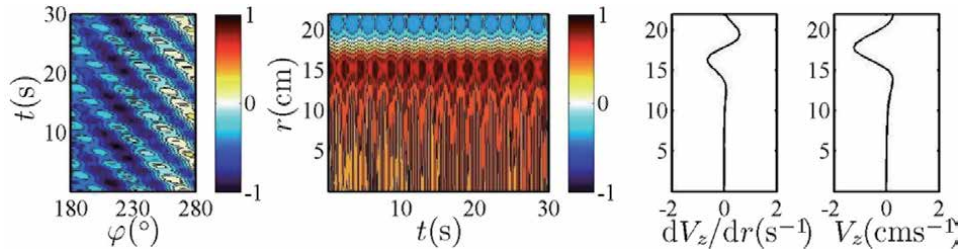

Figure 4.
From left to right: Azimuthal Hovmöller diagram of the stream function ψ with the radius of the maximum radial shear chosen as the reference radius; radial Hovmöller diagram of ψ averaged azimuthally in the range forced sector; radial shear profiles of the azimuthal velocity V_z averaged azimuthally in the same sector and in time.

azimuthal (φ-t) Hovmöller diagram of ψ, the radial t-r Hovmöller diagram of ψ, the radial profiles of the mean radial shear $d\langle \overline{V_Z} \rangle_\varphi/dr$ and the mean azimuthal velocity $\langle \overline{V_Z} \rangle_\varphi$. The profiles show a maximum of the mean zonal velocity in correspondence of the radius r_C corresponding to the jet centerline while the maximum of the mean shear is at a radius $r_{MS} > r_C$. We recall that the definition of the jet boundaries and of its time evolution is crucial in the definition of the barriers to meridional transport [5, 13].
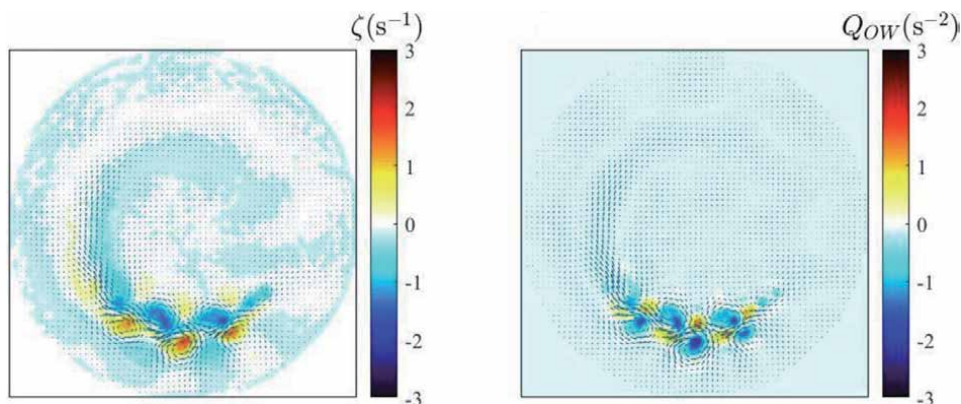
Figure 5.
Instantaneous fields of vorticity field ζ (left) and Okubo–Weiss parameter Q_{ow} (right); velocity field superimposed (blue arrows) for a WW flow.

As discussed in Section 3.1, by measuring the slope of the lines of the same color, we were able to estimate experimentally the speed of the propagating structures relative to the zonal flow with Eq. (2); we then calculate the theoretical speed using Eq. (3) and compare the obtained values. The comparison shows that the relative error, i.e. the ratio between the measured and the expected speed, is minimum in correspondence of r_{MS} ($O(10^{-2})$).

In order to compare our method to evaluate the eddies propagation speed with a method widely used in the applications we also applied an OW-based method to our experimental data sets. At first, we evaluated OW parameter through Eq. (4) at each time instant. Then, using a threshold of $OW_0 = 0.5\sigma_{OW}$ we identified the vortex cores and their surrounding area. We refined the detection by combining the OW parameter with the physical properties of the flow field (high vorticity areas, velocity vectors) and by applying geometrical constraints. An example is provided in **Figure 5** in which we show a snapshot of the vorticity field ζ (left) and of the Okubo–Weiss parameter Q_{OW} (right) superimposed on the corresponding velocity field. In the vorticity map, regions of dark blue (dark red) identify strong anti-cyclonic (cyclonic) circulation. In the Q_{ow} field, dark blue identifies regions where vorticity is much stronger than strain (i.e., eddy cores), and dark red where strain is much greater than vorticity.

Finally, once identified the coherent vortices, we detected the center of each structure and tracked them in the considered time interval. We found values of the propagating speed close to the ones found through the Hovmöller diagrams. We conclude that waves and propagating eddies coexist in the zonal pattern and confirm their duality nature [14]. The application of the same procedure of analysis overall the EW experiments is actually in progress [38].

4.1.2 Characteristic scales and flow regime

The estimation of flow characteristic length scales is crucial to identify the flow regime in rotating turbulent flows with a β-effect. To this aim, as discussed in Section 2.1, we calculate the Rhines number, k_{RH}, the transitional wave number, k_{β}, and their ratio R_β. The results for a set of WW and EW experiments are reported in **Table 1**.

According to the classification provided in [8] we conclude that all our experiments reproduced flows in a transitional regime.

Run	k_{Rh} (cm^{-1})	k_β (cm^{-1})	R_β
WW$_1$	1.41	2.20	1.55
WW$_2$	1.09	1.75	1.60
WW$_3$	0.94	1.16	1.70
EW$_1$	1.19	1.90	1.59
EW$_2$	0.85	1.45	1.70
EW$_3$	0.74	1.29	1.75

Table 1.
Characteristic scales and zonostrophy index estimated from experimental data.

4.2 Flow patterns in the left ventricle downstream of prosthetic valves

To perform flow measurements in the LV, the vertical symmetry plane aligned with the mitral and aortic valve axes is illuminated by a 12 W, infrared laser. The working fluid inside the ventricle (distilled water) is seeded with neutrally buoyant particles ($d_m \sim 30$ μm). A high-speed digital camera (250 frames/s, 1280 × 1024 pixel resolution) is triggered by the motor to frame the time evolution of the phenomenon for N cardiac cycles. The acquired images are processed by means of a FT algorithm and velocity fields on a regular grid 51 × 51 are obtained for the considered time interval. Two-dimensional Eulerian velocity data were then phase averaged over N = 50 cycles. Here, we discuss two groups of experiments performed considering a period T = 6 s and stroke volumes SV_1 = 64 ml, SV_2 = 80 ml. We briefly recall that during the cardiac cycle the flow rate change according to the considered law [21]: the fluid enters the LV through the mitral valve during the diastole (0.00 T – 0.75 T) and is ejected out through the aortic valve during the systole (0.75 T – 1.00 T). Two peaks separated by the diastasis characterize the diastole phase: the first is called E-wave and corresponds to the dilation of the ventricle, and the second, called A-wave, is due to the contraction of the left atrium.

For the dynamic similarity, we consider the Reynolds number $Re = UD/\upsilon$ and the Womersley number $Wo = \sqrt{D^2/T\upsilon}$; respectively equal to Re_1 = 8322; Re_2 = 10403; Wo = 22.8; in both cases within the physiological range. Here, D is the maximum diameter of the ventricle, U the peak velocity through the mitral orifice, ν the kinematic viscosity of the working fluid i.e., distilled water.

We use the public domain code NEWMAN [39] to compute the FTLEs from the planar velocity dataset above described, for the details see [40]. We remark that FTLE fields are computed from 2D measurements even if it is well known that the observed phenomenon is 3D; indeed, as the measurement plane is a plane of symmetry the assumption of two-dimensionality is quite acceptable.

Figure 6 shows backward FTLE at the end of the E-wave for the three simulated conditions. Backward FTLE ridges correspond to the front of the diastolic jet, sharply separating the fluid which just entered the ventricle from the receiving fluid.

The analysis of the FTLE patterns throughout the cardiac cycle (not shown here) highlights how in the physiological configuration the observed coherent structures appear to be optimal for the systolic function. Indeed, the modifications in the transmitral flow due to the presence of a prosthetic valve deeply impact on the interaction between the coherent structures generated during the first phase of the diastole and the incoming jet during the second diastolic phase. We observed that
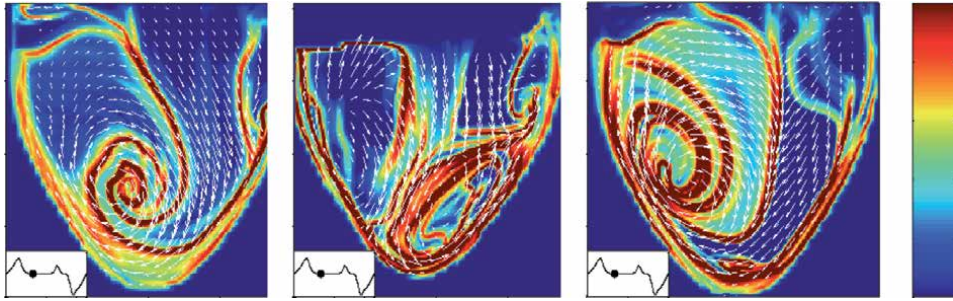
Figure 6.
Velocity fields and backward FTLE at the end of E-wave (the small inset shows the current time in the cardiac cycle as a black dot): Left: Physiological configuration, center: Monoleaflet valve, and right: Bileaflet valve.

while the flow generated by a bileaflet valve preserves most of the beneficial features of the top hat inflow, downstream of a monoleafleat one the strong jet forming at the end of the diastole prevents the permanence of large coherent structures within the LV (**Figure** 7).

In order to complete the FTLE analysis, we reconstruct the trajectories of a number ($O(10^4)$) of synthetic fluid particles entering the ventricle through the mitral orifice during the LV filling by numerically integrating the experimental velocity fields; for each run, synthetic particles were released during each time step of the diastolic waves from the mitral orifice section and were subsequently tracked during the cardiac cycle. The aim was to further clarify the role of LCS by overlapping the
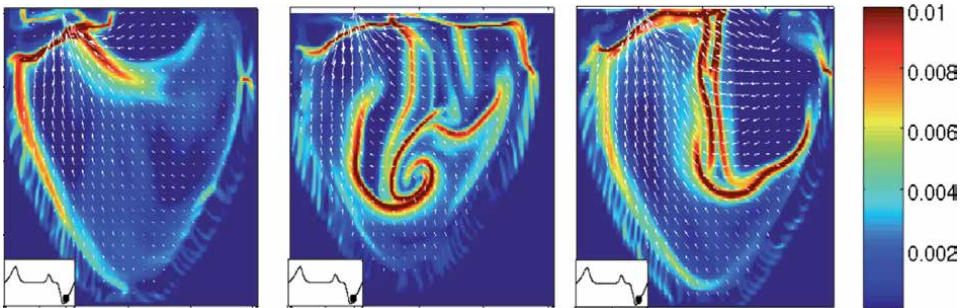

Figure 7.
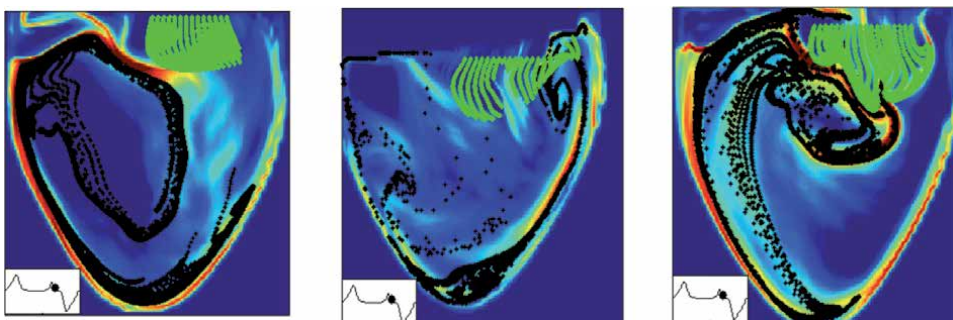*Same as above in correspondence of the systolic peak.*

Figure 8.
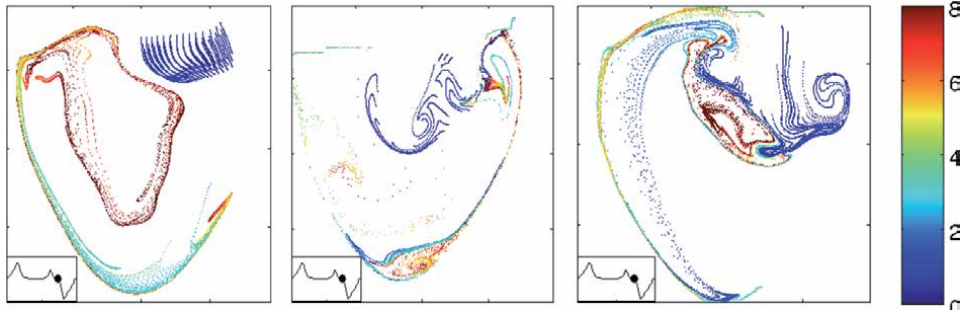*Syntetic particles overlapped on FTLE maps at the end of the a wave.*

Figure 9.
Synthetic particles entered through the mitral orifice during diastolic waves colored according to the shear stress cumulated until the end of the A-wave (the color bar values correspond to the non-dimensional maximum shear stress).

particle positions on the FTLE maps, and to verify if and how LCS may act as pseudo-barriers for transport and mixing. An example is reported in **Figure 8**.

We finally compute the shear stress experienced by the particles along their trajectories in order to emphasize the differences among the simulated conditions and to clarify the possible implications on the hemodynamics. Results corresponding to the end of the A wave are shown in **Figure 9**.

The plots show that, in case (a) the stress magnitudes induced by the smoother flow pattern are lower than values measured in case (b) and (c). In fact, while in physiological conditions particles characterized by the highest shear are washed out by the systolic wave, in presence of prosthetic valves they tend to be advected towards regions of the LV not affected by the systolic ejection (see **Figure 3**).

5. Conclusions

In this work, we review a set of methodologies suitable for the characterization of time-periodic complex flows; in particular, here, the focus is on rotating flows affected by a β-effect and blood flow in the left ventricle. The interest in deepening these contexts depends on their importance from both an applicative and a method-ological point of view. Indeed, we consider almost 2D and time-periodic flows in which, due to chaotic advection, the Lagrangian motion of passive particles can be very complex even in regular, i.e., non-turbulent, Eulerian flow fields. We believe that the obtained results show, on one hand, that the designed experimental models prove suitable to reproduce the investigated phenomena, and on the other hand confirm that the proposed methodologies represent valid and powerful tools for identifying and characterizing the main flow patterns in their space–time evolution.

Acknowledgements

Conflict of interest

The authors declare no conflict of interest.

Author details

Stefania Espa[1*], Maria Grazia Badas[2] and Simon Cabanes[1]

1 Sapienza University of Rome, Rome, Italy

2 University of Cagliari, Cagliari, Italy

*Address all correspondence to: stefania.espa@uniroma1.it

IntechOpen

References

[1] Crisanti A, Falcioni M, Paladin G, Vulpiani A. Lagrangian chaos:Transport, mixing and diffusion in fluids. La Rivista del Nuovo Cimento. 1991;**14**: 1-80. DOI: 10.1007/BF02811193

[2] Rhines PB. Waves and turbulence on a beta-plane. Journal of Fluid Mechanics. 1975;**69**:417-443. 69(3), 417-443. DOI: 10.1017/S0022 112075001504

[3] Cho JYK, Polvani LM. The emergence of jets and vortices in freely evolving, shallow-water turbulence on sphere. Physics of Fluids. 1996;**8**: 1531-1552. DOI: 10.1063/1.868929

[4] Maximenko NA, Bang B, Sasaki H. Observational evidence of alternating zonal jets in the World Ocean. Geophysical Research Letters. 2005;**32**: L12607. DOI: 10.1029/2005GL022728

[5] Galperin B, Read PL (Eds.). Zonal Jets: Phenomenology, Genesis, and Physics. Cambridge University Press; 2019. p. 550. DOI: 10.1017/ 9781107358225

[6] Galperin B, Sukoriansky S, Dikovskaya N. Geophysical flows with anisotropic turbulence and dispersive waves: Flows with a β-effect. Ocean Dynamics. 2010;**60**:427-441. DOI: 10.1007/s10236-010-0278-2

[7] Kraichnan RH. Inertial ranges in two-dimensional turbulence. Physics of Fluids. 1967;**10**:1417. DOI: 10.1063/ 1.1762301

[8] Sukoriansky S, Dikovskaya N, Galperin B. On the arrest of the inverse energy cascade and the Rhines scale. Journal of the Atmospheric Sciences. 2007;**64**:3312-3327. DOI: 10.1175/ JAS4013.1

[9] Espa S, Di Nitto G, Cenedese A. The emergence of zonal jets in forced rotating shallow water turbulence: A laboratory study. Europhysics Letters. 2010;**92**:34006. DOI: 10.1209/ 0295-5075/92/34006

[10] Di Nitto G, Espa S, Cenedese A. Simulating zonation in geophysical flows by laboratory experiments. Physics of Fluids. 2013;**25**:086602. DOI: 10.1063/1.4817540

[11] Derzho OG, Afanasyev YD. Rotating dipolar gyres on a β-plane. Physics of Fluids. 2008;**20**:036603. DOI: 10.1063/ 1.2890083

[12] Galperin B, Hoemann J, Espa S, Di Nitto G. Anisotropic turbulence and Rossby waves in an easterly jet: An experimental study. Geophysical Research Letters. 2014;**41**:6237-6243. DOI: 10.1002/2014gl060767

[13] Galperin B, Hoemann J, Espa S, Di Nitto G, Lacorata G. Anisotropic macroturbulence and diffusion associated with a westward zonal jet: From laboratory to planetary atmospheres and oceans. Physical Review E. 2016;**94**:063102. DOI: 10.1103/PhysRevE.94.063102

[14] Espa S, Cabanes S, King GP, Di Nitto G, Galperin B. Eddy-wave duality in a rotating flow. Physics of Fluids. 2020;**32**:076604. DOI: 10.1063/ 5.0006206

[15] Cabanes S, Espa S, Galperin B, Young RMB, Read PL. Revealing the intensity of turbulent energy transfer in planetary atmospheres. Journal of Geophysical Research. 2020;**47**:2316. DOI: 10.1029/2020GL088685

[16] Pedrizzetti G, Domenichini F. Nature optimizes the swirling flow in the human left ventricle. Physical Review Letters. 2005;**95**:108101. DOI: 10.1103/PhysRevLett.95.108101

[17] Yoganathan AP, He Z, Casey Jones S. Fluid mechanics of heart valves. Annual Review of Biomedical Engineering. 2004;**6**:331-362. DOI: 10.1146/annurev.bioeng.6. 040803.140111

[18] Sotiropoulos F, Le TB, Gilmanov A. Fluid mechanics of heart valves and their replacements. Annual Review of Fluid Mechanics. 2016;**48**:259-283. DOI: 10.1146/annurev-fluid-122414-034314

[19] Querzoli G, Cenedese A, Fortini S. Effect of the prosthetic mitral valve on vortex dynamics and turbulence of the left ventricular flow. Physics of Fluids. 2010;**22**:041901. DOI: 10.1063/ 1.3371720

[20] Fortini S, Querzoli G, Espa S, Cenedese A. Three-dimensional structure of the flow inside the left ventricle of the human heart. Experiments in Fluids. 2013;**54**:1-9. DOI: 10.1007/s00348-013-1609-0

[21] Espa S, Badas MG, Fortini S, Querzoli G, Cenedese A. A Lagrangian investigation of the flow inside the left ventricle. European Journal of Mechanics - B/Fluids. 2012;**35**:9-19. DOI: 10.1016/j.euromechflu.2012.01.015

[22] Moroni M, Cenedese A. Comparison among feature tracking and more consolidated velocimetry image analysis techniques in a fully developed turbulent channel flow. Measurement Science and Technology. 2005;**16**:2307. DOI: b10.1088/0957-0233/16/11/025

[23] Funiciello F, Moroni M, Piromallo C, Faccenna C, Cenedese A, Bui HA. Mapping mantle flow during retreating subduction: Laboratory models analyzed by feature tracking. Journal of Geophysical Research. 2006; **111**:B03402-B03412. DOI: 10.1029/ 2005GL025390

[24] Okubo A. Horizontal dispersion of floatable particles in the vicinity of

velocity singularities such as convergences. Deep Sea Research. 1970; **17**:445-454. DOI: 10.1016/0011-7471 (70)90059-8

[25] Weiss J. The dynamics of enstrophy transfer in two-dimensional hydrodynamics. Physica D. 1991;**48**: 273-294. DOI: 10.1016/0167-2789(91) 90088-Q

[26] Elhmaïdi D, Provenzale A, Babiano A. Elementary topology of two dimensional turbulence from a Lagrangian viewpoint and single-particle dispersion. Journal of Fluid Mechanics. 1993;**257**:533-558. DOI: 10.1017/S0022112093003192

[27] Pasquero C, Provenzale A, Babiano A. Parameterization of dispersion in two-dimensional turbulence. Journal of Fluid Mechanics. 2001;**439**:279-303. DOI: 10.1017/ S0022112001004499

[28] Shadden SC, Lekien F, Marsden JE. Definition and properties of Lagrangian coherent structures from finite-time Lyapunov exponents in two-dimensional aperiodic flows. Physica D: Nonlinear Phenomena. 2005;**212**: 271-304. DOI: 10.1016/j.physd.2005. 10.007

[29] Beron-Vera FJ, Olascoaga M, Goni G. Oceanic mesoscale eddies as revealed by Lagrangian coherent structures. Geophysical Research Letters. 2008;**35**:12. DOI: 10.1029/ 2008GL033957

[30] Haller G. Distinguished material surfaces and coherent structures in three-dimensional fluid flows. Physica D. 2001;**149**:248-277. DOI: 10.1016/S0167-2789(00)00199-8

[31] Haller G. Lagrangian coherent structures. Annual Review of Fluid Mechanics. 2015;**47**:137-162. DOI: 10.1146/annurev-fluid-010313-141322

[32] Shadden SC, Taylor CA. Characterization of coherent structures in the cardiovascular system. Annals of Biomedical Engineering. 2008;**36**(7): 1152-1162. DOI: 10.1007/s10439-008-9502-3

[33] Miron P, Vétel J, Garon A. On the use of the finite-time Lyapunov exponent to reveal complex flow physics in the wake of a mechanical valve. Experiments in Fluids. 2014;**55**: 1-15. DOI: 10.1007/s00348-014-1814-5

[34] Hendabadi S, Bermejo J, Benito Yotti R, Fernández-Avilés F, del Álamo JC, Shadden SC. Topology of blood transport in the human left ventricle by novel processing of Doppler echocardiography. Annals of Biomedical Engineering. 2013;**41**:2603-2616. DOI: 10.1007/s10439-013-0853-z

[35] Bermejo J, Benito Y, Alhama M, Yotti R, Martínez-Legazpi P, Del Villar CP, et al. Intraventricular vortex properties in nonischemic dilated cardiomyopathy. AJP - Heart and Circulatory Physiology. 2014;**306**: H718-H729. DOI: 10.1152/ajpheart. 00697.2013

[36] Badas MG, Domenichini F, Querzoli G. Quantification of the blood mixing in the left ventricle using finite time Lyapunov exponents. Meccanica. 2017;**52**(3):529-544. DOI: 10.1007/ s11012-016-0364-8

[37] Di Labbio G, Vétel J, Kadem L. Material transport in the left ventricle with aortic valve regurgitation. Physical Review Fluids. 2021;**6**:059901. DOI: 10.1103/PhysRevFluids.6.059901

[38] Espa S, Cabanes S. Eddies and waves in a rotating flow: An experimental study. In: Proceedings of the 39th IAHR World Congress 19–24 June 2022, Granada, Spain

[39] Du Toit PC, Marsden JE. Horseshoes in hurricanes. Journal of Fixed Point Theory and Applications 2010;**7**(2):351-384. DOI: 10.1007/s11784-010-0028-6.

[40] Badas MG, Espa S, Fortini S, Querzoli G. 3D finite time Lyapunov exponents in a left ventricle laboratory model. EPJ Web of Conferences. 2015; **926**:02004. DOI: 10.1051/epjconf/ 20159202004

Edited by İlkay Bakırtaş and Nalan Antar

This book discusses vortex dynamics theory from physics, mathematics, and engineering perspectives. It includes nine chapters that cover a variety of research results related to vortex dynamics including nonlinear optics, fluid dynamics, and plasma physics.